Proceedings 10th NUMGE 2023
10th European Conference on Numerical Methods in Geotechnical Engineering
Zdravkovic L, Kontoe S, Taborda DMG, Tsiampousi A (eds)

https://doi.org/10.53243/NUMGE2023-439

Finite element limit analysis using higher-order elements

C.M. Martin

Department of Engineering Science, University of Oxford, Oxford, UK

ABSTRACT: For more than 50 years it has been known that the classical lower and upper bound theorems of plasticity can be implemented by means of the finite element method. Finite element limit analysis, as it is known, gives rise to optimisation problems that typically involve a large but sparse system of linear constraints, supplemented by numerous nonlinear constraints that are needed to enforce the yield restriction (in lower bound analysis) or the associated flow rule (in upper bound analysis). For many common yield criteria, the nonlinear constraints can be expressed in a form that is compatible with standard classes of optimisation such as second-order cone programming and semidefinite programming, for which specialised solvers are available. Historically, particularly for lower bound analysis, linear finite elements have been used to interpolate the fundamental field variables. This paper outlines the formulation and implementation of higher-order stress elements for lower bound analysis and higher-order velocity elements for upper bound analysis, highlighting the recent emergence of Bernstein basis polynomials as an alternative to the Lagrange basis polynomials that are conventionally used for finite elements.

Keywords: plasticity; limit analysis; lower bound; upper bound; finite element

1 INTRODUCTION

Finite element limit analysis (FELA) is a numerical method that seeks to apply the lower bound (LB) and upper bound (UB) theorems of plasticity to boundary value problems by solving the constrained optimisation problems that arise from finite element discretisations of the relevant field variables.

In limit analysis, the loaded structure is assumed to be made of an idealised rigid, perfectly plastic (infinitely ductile) material. The set of plastically admissible stresses – those at or below yield – is here denoted K. In general, the strength properties may vary with position, such that $K = K(\mathbf{x})$. The structure V is subject to body forces $\mathbf{b}$ and its boundary surface $S = \partial V$ is partitioned into S_u and S_t, with a fixed support condition $\mathbf{u} = \mathbf{0}$ applied to S_u and surface tractions $\mathbf{t}$ prescribed on S_t. For $\mathbf{b}$ and $\mathbf{t}$ it is convenient to assume proportional loading, in which a set of dead loads is incrementally modified (in a quasi-static manner) by the action of a scalar load multiplier β on a reference set of live loads:

$$\mathbf{b} = \mathbf{b}^{\text{dead}} + \beta\mathbf{b}^{\text{live}}$$
$$\mathbf{t} = \mathbf{t}^{\text{dead}} + \beta\mathbf{t}^{\text{live}}$$

If the rigid–plastic material obeys the postulate of maximum plastic dissipation (which holds if and only if K is convex and the strain rate $\boldsymbol{\varepsilon}$ at yield exhibits associated flow (normality) with respect to K), and if all changes in geometry occurring during collapse are neglected, the theorems of limit analysis established by Drucker et al. (1952) can be used to obtain strict bounds β^- and β^+ on the exact collapse load multiplier β^*.

The goal of LB FELA is to compute a lower bound load multiplier $\beta^- \le \beta^*$ by constructing a stress field $\boldsymbol{\sigma}$ that satisfies (a) the equations of equilibrium, both within and (if the stress field is discontinuous) between elements; (b) the stress boundary conditions; (c) the continuum yield restriction $\boldsymbol{\sigma} \in K$, typically expressed in the form $f(\boldsymbol{\sigma}) \le 0$ where f is the yield function. In some problems it is also necessary to apply an interface yield restriction $f(\mathbf{t}) \le 0$ to the traction field $\mathbf{t}$ that is developed on certain edges/faces of the mesh. For a given finite element discretisation, the stress field is adjusted to maximise β^-.

The goal of UB FELA is to compute an upper bound load multiplier $\beta^+ \ge \beta^*$ by constructing a kinematically admissible velocity field $\mathbf{u}$ and evaluating

$$\beta^+ = \frac{W_{\text{int}}(\boldsymbol{\varepsilon}) - W_{\text{ext}}^{\text{dead}}(\mathbf{u})}{W_{\text{ext}}^{\text{live}}(\mathbf{u})}$$

where $\boldsymbol{\varepsilon}$ is the strain rate field induced by the velocity field, W_{int} is the internal work (plastic dissipation) rate, and $W_{\text{ext}}^{\text{dead}}$ and $W_{\text{ext}}^{\text{live}}$ are the external work rates of the dead and live loads. The strain rate $\boldsymbol{\varepsilon}$ is constrained to comply with the continuum associated flow rule, and $W_{\text{int}}(\boldsymbol{\varepsilon})$ is found by integrating the dissipation function $D(\boldsymbol{\varepsilon})$ over every element:

$$W_{\text{int}}(\boldsymbol{\varepsilon}) = \int D(\boldsymbol{\varepsilon})\, dV, \quad D(\boldsymbol{\varepsilon}) = \sup_{\boldsymbol{\sigma}\in K}(\sigma_{ij}\varepsilon_{ij})$$

If the velocity field is allowed to be discontinuous across certain edges/faces of the mesh, the velocity jumps $\Delta\mathbf{u}$ are constrained to comply with the interface associated

flow rule, and an additional dissipation term $W_{\text{int}}(\Delta\mathbf{u})$ needs to be included (see e.g. Makrodimopoulos and Martin, 2008; Salençon, 1983). For a given finite element discretisation, the velocity field is adjusted to minimise β^+.

This paper describes the formulation of various finite elements that can be used to perform FELA of solid structures in 2D and 3D, with particular emphasis on higher-order elements. The main focus is on providing an outline of the underlying theory, but the performance of the elements is also evaluated for a small selection of geotechnical benchmark problems.

2 ELEMENT TYPES

The finite elements used in FELA typically interpolate stress or velocity over a simplex (line segment, triangle, or tetrahedron), with the interpolation being performed using Lagrange polynomials or Bernstein polynomials. Elements based on Lagrange polynomials are ubiquitous in implementations of the displacement finite element method, and detailed descriptions of their formulation can be found in many textbooks (e.g. Cook et al., 2002; Zienkiewicz et al., 2005). Elements based on Bernstein (or Bernstein-Bézier) polynomials are not so commonly encountered in engineering, but this interpolation scheme is widely used in fields such as numerical analysis and computer-aided geometric design (see e.g. Farouki, 2012; Lai and Schumaker, 2007; Prautzsch et al., 2002). Bernstein elements turn out to be particularly well suited to the demands of obtaining strict LB and UB solutions in FELA, as discussed in two recent papers by Makrodimopoulos (2020, 2022).

This paper focuses on triangular elements (and their line segment edges), though the formulations given can readily be generalised to tetrahedral elements (and their triangular faces). The interpolating polynomials are expressed in terms of the normalised barycentric coordinates defined in Figure 1: length coordinates $\boldsymbol{l}$, area coordinates $\boldsymbol{a}$, and volume coordinates $\boldsymbol{v}$. The degree of the interpolating polynomials is denoted N, with $N \geq 0$. The number of basis polynomials required to provide a complete polynomial interpolation is $N+1$ for a line segment, $(N+1)(N+2)/2$ for a triangle, and $(N+1)(N+2)(N+3)/6$ for a tetrahedron. The first few triangular elements are shown in Figure 2, indicating both nodes and 'derivative points' (these coincide with the nodes of the previous element, and will be discussed later).

For a line segment, the *i*th basis polynomial of degree N will be denoted $h_i^{(l,N)}$, with the complete set of such polynomials being denoted $\boldsymbol{h}^{(l,N)}$. Similar notation will be used to refer to the basis polynomials for a triangle ($h_i^{(a,N)}$, $\boldsymbol{h}^{(a,N)}$) and a tetrahedron ($h_i^{(v,N)}$, $\boldsymbol{h}^{(v,N)}$). From the context it will be clear whether Lagrange or Bernstein polynomials are being used.

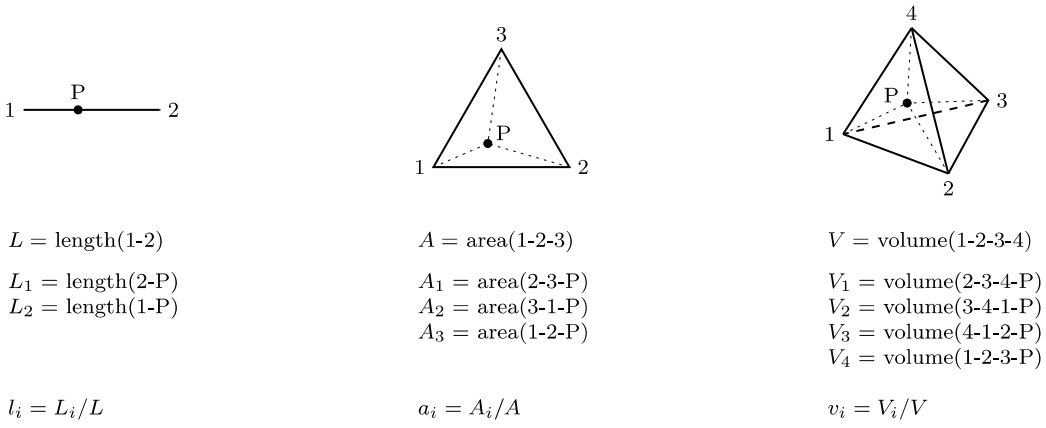

Figure 1. Definitions of length coordinates $\boldsymbol{l}$, area coordinates $\boldsymbol{a}$, and volume coordinates $\boldsymbol{v}$

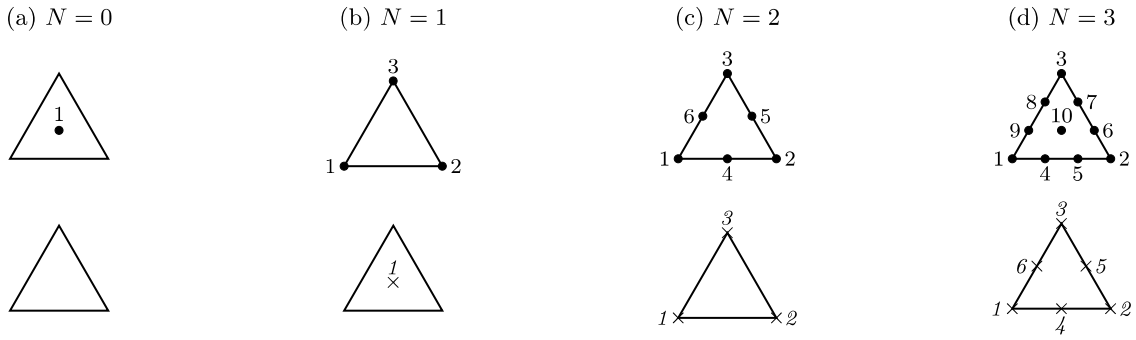

Figure 2. Nodes (circles) and derivative points (crosses) for triangular elements of various orders N

2.1 Lagrange polynomials

For a line segment, assuming equally spaced nodes, the first few sets of Lagrange basis polynomials in terms of length coordinates are

$$\boldsymbol{h}^{(l,0)} = \{1\}$$
$$\boldsymbol{h}^{(l,1)} = \{l_1, l_2\}$$
$$\boldsymbol{h}^{(l,2)} = \left\{2l_1\left(l_1 - \tfrac{1}{2}\right), 2l_2\left(l_2 - \tfrac{1}{2}\right), 4l_1l_2\right\}$$
$$\boldsymbol{h}^{(l,3)} = \begin{Bmatrix} \tfrac{9}{2}l_1\left(l_1 - \tfrac{1}{3}\right)\left(l_1 - \tfrac{2}{3}\right), \tfrac{9}{2}l_2\left(l_2 - \tfrac{1}{3}\right)\left(l_2 - \tfrac{2}{3}\right), \\ \tfrac{27}{2}l_1l_2\left(l_1 - \tfrac{1}{3}\right), \tfrac{27}{2}l_1l_2\left(l_2 - \tfrac{1}{3}\right) \end{Bmatrix}$$

These basis polynomials provide a partition of unity ($\sum_{i=1}^{N+1} h_i^{(l,N)} = 1$) for any value of N, but they are only non-negative ($h_i^{(l,N)} \geq 0\ \forall i$) for $N = 0$ and $N = 1$.

For a triangle, the first few sets of Lagrange basis polynomials in terms of area coordinates are

$$\boldsymbol{h}^{(a,0)} = \{1\}$$
$$\boldsymbol{h}^{(a,1)} = \{a_1, a_2, a_3\}$$
$$\boldsymbol{h}^{(a,2)} = \begin{Bmatrix} 2a_1\left(a_1 - \tfrac{1}{2}\right), 2a_2\left(a_2 - \tfrac{1}{2}\right), 2a_3\left(a_3 - \tfrac{1}{2}\right), \\ 4a_1a_2, 4a_2a_3, 4a_3a_1 \end{Bmatrix}$$
$$\boldsymbol{h}^{(a,3)} = \begin{Bmatrix} \tfrac{9}{2}a_1\left(a_1 - \tfrac{1}{3}\right)\left(a_1 - \tfrac{2}{3}\right), \ldots, \tfrac{9}{2}a_3\left(a_3 - \tfrac{1}{3}\right)\left(a_3 - \tfrac{2}{3}\right), \\ \tfrac{27}{2}a_1a_2\left(a_1 - \tfrac{1}{3}\right), \ldots, \tfrac{27}{2}a_3a_1\left(a_1 - \tfrac{1}{3}\right), \\ 27a_1a_2a_3 \end{Bmatrix}$$

Again, these basis polynomials provide a partition of unity for any value of N, but they are only non-negative for $N = 0$ and $N = 1$.

Following the usual convention of finite element analysis, the basis polynomials in each set are ordered hierarchically, e.g. the set $\boldsymbol{h}^{(a,3)}$ for cubic interpolation over a triangle is ordered with the three 'vertex' polynomials first, then the six 'edge' polynomials, then the one 'interior' polynomial (as per Figure 2(d)).

2.2 Lagrange elements

Figure 3 shows graphs of the first few sets of Lagrange basis polynomials for a line segment, together with the corresponding 1D Lagrange elements. The Kronecker delta property – the *i*th basis polynomial being equal to 1 at node i and 0 at all other nodes – is satisfied for elements of any order N. Interpolation of a variable u with nodal values u_i is performed using

$$u = \sum_{i=1}^{N+1} h_i^{(l,N)} u_i$$

Corresponding 2D Lagrange elements can be developed using basis polynomials from the sets $\boldsymbol{h}^{(a,N)}$ above.

When a 2D Lagrange element is used to interpolate a variable u, the basis polynomials are such that the variation of u along an edge of the triangle is completely defined by the nodes lying along that edge. Furthermore, this variation can be reproduced using a 1D Lagrange element of the same order N.

2.3 Bernstein polynomials

For a line segment, the first few sets of Bernstein basis polynomials in terms of length coordinates are

$$\boldsymbol{h}^{(l,0)} = \{1\}$$
$$\boldsymbol{h}^{(l,1)} = \{l_1, l_2\}$$
$$\boldsymbol{h}^{(l,2)} = \{l_1^2, l_2^2, 2l_1l_2\}$$
$$\boldsymbol{h}^{(l,3)} = \{l_1^3, l_2^3, 3l_1^2l_2, 3l_1l_2^2\}$$

These basis polynomials provide a partition of unity ($\sum_{i=1}^{N+1} h_i^{(l,N)} = 1$) and are non-negative ($h_i^{(l,N)} \geq 0\ \forall i$) for any value of N. For a general N, the polynomials are given by the formula

$$b_{mn}^{(N)}(\boldsymbol{l}) = \frac{N!}{m!n!} l_1^m l_2^n$$

with $m, n \geq 0$ and $m + n = N$.

For a triangle, the first few sets of Bernstein basis polynomials in terms of area coordinates are

$$\boldsymbol{h}^{(a,0)} = \{1\}$$
$$\boldsymbol{h}^{(a,1)} = \{a_1, a_2, a_3\}$$
$$\boldsymbol{h}^{(a,2)} = \{a_1^2, a_2^2, a_3^2, 2a_1a_2, 2a_2a_3, 2a_3a_1\}$$
$$\boldsymbol{h}^{(a,3)} = \{a_1^3, a_2^3, a_3^3, 3a_1^2a_2, \ldots, 3a_3a_1^2, 6a_1a_2a_3\}$$

Again, these basis polynomials provide a partition of unity and are non-negative for any value of N. For a general N, the polynomials are given by the formula

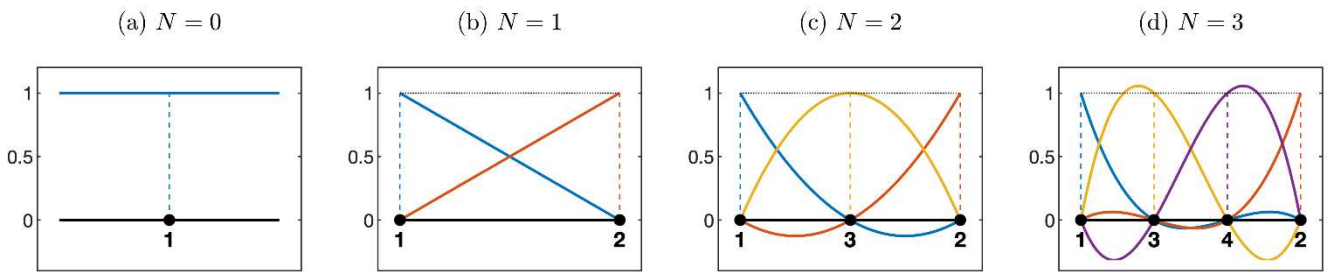

Figure 3. Lagrange basis polynomials (colours) and corresponding 1D Lagrange elements (black)

$$b_{lmn}^{(N)}(\boldsymbol{a}) = \frac{N!}{l!m!n!} a_1^l a_2^m a_3^n$$

with $l, m, n \geq 0$ and $l + m + n = N$.

Another interesting property of Bernstein basis polynomials is that when they are integrated over the relevant simplex, the integral of each polynomial in a given set is the same. When $N = 3$, for example,

$$\int h_i^{(l,3)} dL = \frac{L}{4} \quad \forall i \in \{1, \ldots, 4\} \tag{1a}$$

$$\int h_i^{(a,3)} dA = \frac{A}{10} \quad \forall i \in \{1, \ldots, 10\} \tag{1b}$$

2.4 Bernstein elements

Figure 4 shows graphs of the first few sets of Bernstein basis polynomials for a line segment, together with the corresponding 1D Bernstein elements. The nodes of each Bernstein element are considered to be located at the (equally spaced) points where the basis polynomials are maximised. Although the Kronecker delta property is only satisfied for $N = 0$ and $N = 1$, a variable u can still be interpolated for any value of N using

$$u = \sum_{i=1}^{N+1} h_i^{(l,N)} u_i^*$$

where u_i^* is the 'nodal weight' applied to the ith basis polynomial $h_i^{(l,N)}$ from the set $\boldsymbol{h}^{(l,N)}$. Because Bernstein basis polynomials provide a partition of unity and are non-negative, the interpolated value of u at any point along the line segment is always a *convex combination* of the nodal weights u_i^*:

$$u = \alpha_1 u_1^* + \cdots + \alpha_{N+1} u_{N+1}^*$$

where the coefficients α_i satisfy the twin conditions

$$\alpha_1 + \cdots + \alpha_{N+1} = 1, \quad \alpha_i \geq 0 \ \ \forall i \in \{1, \ldots, N+1\}$$

Corresponding 2D Bernstein elements can be developed using basis polynomials from the sets $\boldsymbol{h}^{(a,N)}$ above.

When a 2D Bernstein element is used to interpolate a variable u, the basis polynomials are such that the variation of u along an edge of the triangle is completely defined by the nodes lying along that edge. Furthermore, this variation can be reproduced using a 1D Bernstein element of the same order N.

For the 1D Bernstein elements shown in Figure 4, the actual nodal values u_i of the interpolated variable u are related to the nodal weights u_i^* as follows:

$$[u_1] = [1][u_1^*] \qquad (N = 0\text{: constant})$$

$$\begin{bmatrix} u_1 \\ u_2 \end{bmatrix} = \begin{bmatrix} 1 & 0 \\ 0 & 1 \end{bmatrix} \begin{bmatrix} u_1^* \\ u_2^* \end{bmatrix} \qquad (N = 1\text{: linear})$$

$$\begin{bmatrix} u_1 \\ u_2 \\ u_3 \end{bmatrix} = \begin{bmatrix} 1 & 0 & 0 \\ 0 & 1 & 0 \\ \frac{1}{4} & \frac{1}{4} & \frac{1}{2} \end{bmatrix} \begin{bmatrix} u_1^* \\ u_2^* \\ u_3^* \end{bmatrix} \qquad (N = 2\text{: quadratic})$$

$$\begin{bmatrix} u_1 \\ u_2 \\ u_3 \\ u_4 \end{bmatrix} = \begin{bmatrix} 1 & 0 & 0 & 0 \\ 0 & 1 & 0 & 0 \\ \frac{8}{27} & \frac{1}{27} & \frac{4}{9} & \frac{2}{9} \\ \frac{1}{27} & \frac{8}{27} & \frac{2}{9} & \frac{4}{9} \end{bmatrix} \begin{bmatrix} u_1^* \\ u_2^* \\ u_3^* \\ u_4^* \end{bmatrix} \qquad (N = 3\text{: cubic})$$

From these equations it is clear that for higher-order ($N \geq 2$) elements based on Bernstein polynomials, the application of Dirichlet (prescribed u) boundary conditions is not quite as straightforward as it is for conventional higher-order elements based on Lagrange polynomials, which satisfy the Kronecker delta property by construction for any degree of interpolation N.

A specific situation that is often encountered in FELA involves determining the nodal weights u_i^* that give rise to a prescribed linear variation of u along a 1D Bernstein element, say from $u = U_1$ at end 1 to $u = U_2$ at end 2. When $N = 1$, the required nodal weights are evidently $u_1^* = U_1$ and $u_2^* = U_2$. When $N = 2$, the actual nodal values are $u_1 = U_1, u_2 = U_2, u_3 = (U_1 + U_2)/2$, so the required nodal weights are

$$\begin{bmatrix} u_1^* \\ u_2^* \\ u_3^* \end{bmatrix} = \begin{bmatrix} 1 & 0 & 0 \\ 0 & 1 & 0 \\ \frac{1}{4} & \frac{1}{4} & \frac{1}{2} \end{bmatrix}^{-1} \begin{bmatrix} 1 & 0 \\ 0 & 1 \\ \frac{1}{2} & \frac{1}{2} \end{bmatrix} \begin{bmatrix} U_1 \\ U_2 \end{bmatrix} = \begin{bmatrix} 1 & 0 \\ 0 & 1 \\ \frac{1}{2} & \frac{1}{2} \end{bmatrix} \begin{bmatrix} U_1 \\ U_2 \end{bmatrix} = \begin{bmatrix} u_1 \\ u_2 \\ u_3 \end{bmatrix}$$

Similar behaviour is observed for $N = 3$, and for all higher values of N. The surprisingly simple outcome is that, in order to match a prescribed linear variation of u, the required weight u_i^* at any node – not just the two vertex nodes – is equal to u_i (the actual value of u at the location of the node in question, as determined from the prescribed linear variation). The same rule holds when determining the nodal weights u_i^* that give rise to a prescribed linear variation of u over a 1D, 2D, or 3D Bernstein element of any order $N \geq 1$.

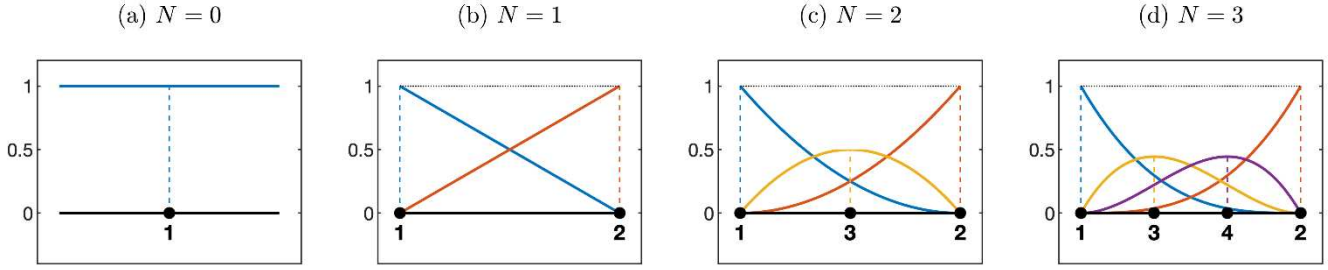

Figure 4. Bernstein basis polynomials (colours) and corresponding 1D Bernstein elements (black)

3 PLANE STRAIN – LOWER BOUND

The 3-node (linear stress, constant stress gradient) triangle is the simplest element capable of providing strict LB solutions for plane strain problems involving body forces. The use of this element dates back to Lysmer (1970) and Pastor (1978); a full review is given by Makrodimopoulos and Martin (2006).

The early LB FELA work by Hodge and Belytschko (1968) and Belytschko and Hodge (1970) was notable for the use of quadratic Lagrange stress elements, but a cumbersome iterative procedure (see Section 3.2.3) was needed to ensure that the yield restriction was satisfied at every point of every element.

Makrodimopoulos (2020) showed that LB FELA can also be performed using Bernstein stress elements, with no limit on the degree of polynomial interpolation, and with no special measures being needed to ensure global compliance with the yield restriction.

In this section, the use of higher-order triangular elements for LB FELA in plane strain will be illustrated in detail for a cubic ($N = 3$) variation of stress. As such, attention will be focused on the 10-node triangle shown in Figure 2(d), considering both Bernstein and Lagrange interpolation schemes.

3.1 Higher-order stress elements (Bernstein)

When cubic Bernstein interpolation is used, the stress field $\boldsymbol{\sigma} = [\sigma_{xx} \;\; \sigma_{yy} \;\; \tau_{xy}]^{\mathrm{T}}$ varies in accordance with

$$\boldsymbol{\sigma} = \sum_{i=1}^{10} h_i^{(a,3)} \boldsymbol{\sigma}_i^* \qquad (2)$$

where $\boldsymbol{\sigma}_i^* = [\sigma_{xx,i}^* \;\; \sigma_{yy,i}^* \;\; \tau_{xy,i}^*]^{\mathrm{T}}$ is the nodal stress weight applied to the ith basis polynomial from the set

$$\boldsymbol{h}^{(a,3)} = \left\{ \begin{matrix} a_1^3, a_2^3, a_3^3, \\ 3a_1^2a_2, 3a_1a_2^2, 3a_2^2a_3, 3a_2a_3^2, 3a_3^2a_1, 3a_3a_1^2, \\ 6a_1a_2a_3 \end{matrix} \right\}$$

as given in Section 2.3.

3.1.1 Continuum equilibrium

For strict intra-element equilibrium in the presence of a body force field $\mathbf{b} = [b_x \;\; b_y]^{\mathrm{T}}$, the equation

$$\mathbf{E}\tilde{\boldsymbol{\sigma}}^* + \mathbf{b} = \mathbf{0} \qquad (3)$$

must hold throughout the element, where

$$\mathbf{E} = \begin{bmatrix} h_{1,x}^{(a,3)} & 0 & h_{1,y}^{(a,3)} & \cdots & h_{10,x}^{(a,3)} & 0 & h_{10,y}^{(a,3)} \\ 0 & h_{1,y}^{(a,3)} & h_{1,x}^{(a,3)} & \cdots & 0 & h_{10,y}^{(a,3)} & h_{10,x}^{(a,3)} \end{bmatrix}$$

(subscripts $,x$ and $,y$ denote partial differentiation) and

$$\tilde{\boldsymbol{\sigma}}^* = [\sigma_{xx,1}^* \;\; \sigma_{yy,1}^* \;\; \tau_{xy,1}^* \;\; \cdots \;\; \sigma_{xx,10}^* \;\; \sigma_{yy,10}^* \;\; \tau_{xy,10}^*]^{\mathrm{T}}$$

To evaluate the partial derivatives in $\mathbf{E}$ it is convenient to take the product of the 10×3 matrix

$$\mathbf{P} = \frac{\partial h_i^{(a,3)}}{\partial a_j} = \begin{bmatrix} 3a_1^2 & 0 & 0 \\ 0 & 3a_2^2 & 0 \\ 0 & 0 & 3a_3^2 \\ 6a_1a_2 & 3a_1^2 & 0 \\ 3a_2^2 & 6a_1a_2 & 0 \\ 0 & 6a_2a_3 & 3a_2^2 \\ 0 & 3a_3^2 & 6a_2a_3 \\ 3a_3^2 & 0 & 6a_3a_1 \\ 6a_3a_1 & 0 & 3a_1^2 \\ 6a_2a_3 & 6a_3a_1 & 6a_1a_2 \end{bmatrix}$$

and the 3×2 matrix

$$\mathbf{Q} = \frac{\partial a_i}{\partial x_j} = \frac{1}{2A} \begin{bmatrix} y_2 - y_3 & x_3 - x_2 \\ y_3 - y_1 & x_1 - x_3 \\ y_1 - y_2 & x_2 - x_1 \end{bmatrix}$$

to obtain the 10×2 matrix

$$\mathbf{PQ} = \frac{\partial h_i^{(a,3)}}{\partial x_j}$$

Since the partial derivatives in $\mathbf{E}$ vary quadratically (this is evident from the quadratic terms in $\mathbf{P}$, noting that $\mathbf{Q}$ is constant), equilibrium can be enforced by direct application of Equation (3) at any six points that are 'quadratically independent', in the sense that

$$\begin{vmatrix} 1 & x_1 & y_1 & x_1^2 & x_1y_1 & y_1^2 \\ 1 & x_2 & y_2 & x_2^2 & x_2y_2 & y_2^2 \\ 1 & x_3 & y_3 & x_3^2 & x_3y_3 & y_3^2 \\ 1 & x_4 & y_4 & x_4^2 & x_4y_4 & y_4^2 \\ 1 & x_5 & y_5 & x_5^2 & x_5y_5 & y_5^2 \\ 1 & x_6 & y_6 & x_6^2 & x_6y_6 & y_6^2 \end{vmatrix} \neq 0$$

The derivative points shown in Figure 2(d) are suitable for this purpose. The equilibrium is strict provided the variation of $\mathbf{b}$ is no more than quadratic.

An alternative approach is to proceed as follows. Let the operation of copying entries from the 10×2 matrix $\mathbf{PQ}$ to populate the 2×30 matrix $\mathbf{E}$ be denoted "$\mathrm{op_E}$":

$$\mathbf{E} = \mathrm{op_E}[\mathbf{PQ}] \qquad (4)$$

Now observe that $\mathbf{P}$ can be decomposed in the form of a quadratic Bernstein interpolation

$$\mathbf{P} = a_1^2\mathbf{P}_1^* + a_2^2\mathbf{P}_2^* + a_3^2\mathbf{P}_3^* + 2a_1a_2\mathbf{P}_4^* + 2a_2a_3\mathbf{P}_5^* + 2a_3a_1\mathbf{P}_6^*$$

where the $\mathbf{P}_i^*$ are constant sparse matrices given by

$$\mathbf{P}_1^* = \begin{bmatrix} 3 & 0 & 0 \\ 0 & 0 & 0 \\ 0 & 0 & 0 \\ 0 & 3 & 0 \\ 0 & 0 & 0 \\ 0 & 0 & 0 \\ 0 & 0 & 0 \\ 0 & 0 & 0 \\ 0 & 0 & 3 \\ 0 & 0 & 0 \end{bmatrix}, \quad \ldots, \quad \mathbf{P}_6^* = \begin{bmatrix} 0 & 0 & 0 \\ 0 & 0 & 0 \\ 0 & 0 & 0 \\ 0 & 0 & 0 \\ 0 & 0 & 0 \\ 0 & 0 & 0 \\ 0 & 0 & 0 \\ 0 & 0 & 3 \\ 3 & 0 & 0 \\ 0 & 3 & 0 \end{bmatrix}$$

Equation (4) can then be elaborated as

$$\mathbf{E} = a_1^2\mathbf{E}_1^* + a_2^2\mathbf{E}_2^* + a_3^2\mathbf{E}_3^* + 2a_1a_2\mathbf{E}_4^* + 2a_2a_3\mathbf{E}_5^* + 2a_3a_1\mathbf{E}_6^*$$

where

$$\mathbf{E}_i^* = \mathrm{op}_\mathrm{E}[\mathbf{P}_i^*\mathbf{Q}]$$

If the variation of the body force field $\mathbf{b}$ is also expressed as a quadratic Bernstein interpolation

$$\mathbf{b} = a_1^2\mathbf{b}_1^* + a_2^2\mathbf{b}_2^* + a_3^2\mathbf{b}_3^* + 2a_1a_2\mathbf{b}_4^* + 2a_2a_3\mathbf{b}_5^* + 2a_3a_1\mathbf{b}_6^*$$

then it follows that enforcing

$$\mathbf{E}_i^*\tilde{\boldsymbol{\sigma}}^* + \mathbf{b}_i^* = \mathbf{0} \quad \forall i \in \{1, \ldots, 6\}$$

will ensure that Equation (3) is satisfied for any set of area coordinates, i.e. throughout the element. If $\mathbf{b}$ is constant, $\mathbf{b}_i^* = \mathbf{b}\ \forall i$. If $\mathbf{b}$ varies linearly then, in view of the discussion at the end of Section 2.4, the body force weights $\mathbf{b}_i^*$ can be obtained by evaluating $\mathbf{b}$ at the six derivative points shown in Figure 2(d).

3.1.2 Interface and boundary equilibrium

In LB FELA it is usual for the discretised stress field to be discontinuous between elements. Figure 5(a) shows two adjacent 2D elements, A and B, with a 1D element of the same order ($N = 3$) embedded along the interface (which has unit normal $\mathbf{n} = [n_x\ n_y]^\mathrm{T}$). If the stress fields $\boldsymbol{\sigma}_\mathrm{A}$ and $\boldsymbol{\sigma}_\mathrm{B}$ have cubic Bernstein interpolations given by Equation (2), the traction vectors $\mathbf{t}_\mathrm{A}$ and $\mathbf{t}_\mathrm{B}$ also have cubic Bernstein interpolations, namely

$$\mathbf{t}_\mathrm{A} = l_1^3\mathbf{t}_{\mathrm{A}1}^* + l_2^3\mathbf{t}_{\mathrm{A}2}^* + 3l_1^2l_2\mathbf{t}_{\mathrm{A}3}^* + 3l_1l_2^2\mathbf{t}_{\mathrm{A}4}^* \quad (5a)$$
$$\mathbf{t}_\mathrm{B} = l_1^3\mathbf{t}_{\mathrm{B}1}^* + l_2^3\mathbf{t}_{\mathrm{B}2}^* + 3l_1^2l_2\mathbf{t}_{\mathrm{B}3}^* + 3l_1l_2^2\mathbf{t}_{\mathrm{B}4}^* \quad (5b)$$

where

$$\mathbf{t}_{\mathrm{A}i}^* = \mathbf{E}_\mathrm{A}\boldsymbol{\sigma}_{\mathrm{A}i}^*$$
$$\mathbf{t}_{\mathrm{B}i}^* = \mathbf{E}_\mathrm{B}\boldsymbol{\sigma}_{\mathrm{B}i}^*$$

with

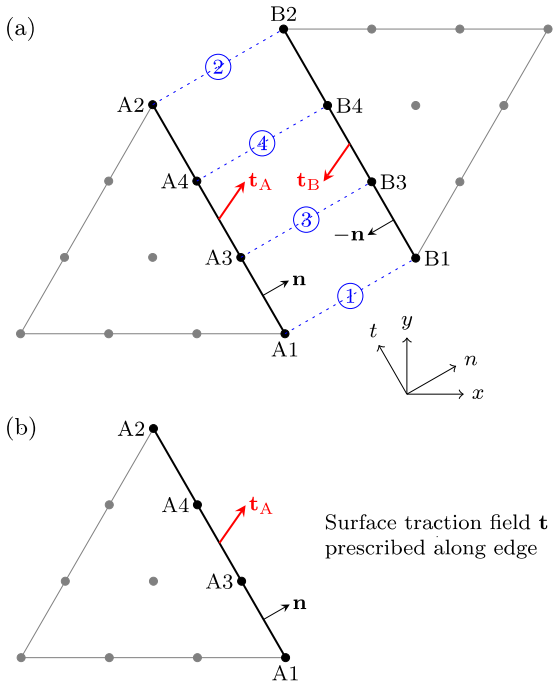

Figure 5. LB FELA with cubic interpolation of stress: (a) inter-element discontinuity; (b) boundary edge

$$\mathbf{E}_\mathrm{A} = \begin{bmatrix} n_x & 0 & n_y \\ 0 & n_y & n_x \end{bmatrix}$$

and $\mathbf{E}_\mathrm{B} = -\mathbf{E}_\mathrm{A}$. For strict inter-element equilibrium the vectors $\mathbf{t}_\mathrm{A}$ and $\mathbf{t}_\mathrm{B}$ must be equal and opposite (such that $\mathbf{t}_\mathrm{A} + \mathbf{t}_\mathrm{B} = \mathbf{0}$) at every point along the interface. From the foregoing equations it is clear that enforcing

$$\mathbf{E}_\mathrm{A}\boldsymbol{\sigma}_{\mathrm{A}i}^* + \mathbf{E}_\mathrm{B}\boldsymbol{\sigma}_{\mathrm{B}i}^* = \mathbf{0} \quad \forall i \in \{1, \ldots, 4\}$$

is sufficient to ensure that $\mathbf{t}_\mathrm{A} + \mathbf{t}_\mathrm{B} = \mathbf{0}$ for any set of length coordinates, i.e. along the whole interface.

A similar approach can be used to ensure strict equilibrium when a surface traction field $\mathbf{t} = [t_x\ \ t_y]^\mathrm{T}$ is prescribed on a boundary edge (Figure 5(b)). If $\mathbf{t}$ can be expressed as a cubic Bernstein interpolation

$$\mathbf{t} = l_1^3\mathbf{t}_1^* + l_2^3\mathbf{t}_2^* + 3l_1^2l_2\mathbf{t}_3^* + 3l_1l_2^2\mathbf{t}_4^*$$

then enforcing

$$\mathbf{E}_\mathrm{A}\boldsymbol{\sigma}_{\mathrm{A}i}^* = \mathbf{t}_i^* \quad \forall i \in \{1, \ldots, 4\}$$

will ensure that $\mathbf{t}_\mathrm{A} = \mathbf{t}$ for any set of length coordinates, i.e. along the whole edge. If $\mathbf{t}$ is constant, $\mathbf{t}_i^* = \mathbf{t}\ \forall i$. If $\mathbf{t}$ varies linearly then, in view of the discussion at the end of Section 2.4, the traction weights $\mathbf{t}_i^*$ can be obtained by evaluating $\mathbf{t}$ at the four nodes of the 1D element.

3.1.3 Continuum yield

The advantage of using Bernstein interpolation in Equation (2) is that at every point in the element, the

interpolated stress $\boldsymbol{\sigma}$ is a convex combination of the nodal stress weights $\boldsymbol{\sigma}_i^*$. This means that if a (convex) continuum yield restriction is applied to each nodal stress weight, it is guaranteed to be satisfied for the interpolated stress throughout the element:

$$f(\boldsymbol{\sigma}_i^*) \le 0 \;\; \forall i \in \{1,\dots,10\} \quad \Rightarrow \quad f(\boldsymbol{\sigma}) \le 0$$

The strength properties can vary with position, but if a strict LB solution is desired then the variation cannot be completely arbitrary. In the case of a Mohr–Coulomb material, the friction angle ϕ must be constant over the element, and the variation of the cohesion c must be expressible as a cubic Bernstein interpolation:

$$c = \sum_{i=1}^{10} h_i^{(a,3)} c_i^*$$

The ith cohesion weight c_i^* is used when applying the yield restriction to the ith nodal stress weight $\boldsymbol{\sigma}_i^*$. In applications it is rare to encounter more than a linear variation of c, so the required cohesion weight c_i^* at any node is usually just equal to c_i (the actual value of c at the location of the node in question) – see Section 2.4.

3.1.4 Interface yield

If an interface yield restriction needs to be applied to some edge of the mesh, the variation of the traction vector $\mathbf{t}$ along the edge is determined (using Equation (5a) – the subscript A is omitted) and expressed as

$$\mathbf{t} = l_1^3 \mathbf{t}_1^* + l_2^3 \mathbf{t}_2^* + 3 l_1^2 l_2 \mathbf{t}_3^* + 3 l_1 l_2^2 \mathbf{t}_4^*$$

The use of Bernstein interpolation means that the interpolated traction $\mathbf{t}$ is a convex combination of the nodal traction weights $\mathbf{t}_i^*$. This in turn means that if a (convex) interface yield restriction is applied to each nodal traction weight, it is guaranteed to be satisfied for the interpolated traction along the whole edge:

$$f(\mathbf{t}_i^*) \le 0 \;\; \forall i \in \{1,\dots,4\} \quad \Rightarrow \quad f(\mathbf{t}) \le 0$$

Again, the strength properties can vary with position; for a Mohr–Coulomb material ϕ must be constant and c must be expressible as a cubic Bernstein interpolation.

3.2 Higher-order stress elements (Lagrange)

When cubic Lagrange interpolation is used, the stress field $\boldsymbol{\sigma} = [\sigma_{xx} \;\; \sigma_{yy} \;\; \tau_{xy}]^{\mathrm{T}}$ varies in accordance with

$$\boldsymbol{\sigma} = \sum_{i=1}^{10} h_i^{(a,3)} \boldsymbol{\sigma}_i \qquad (6)$$

where $\boldsymbol{\sigma}_i = [\sigma_{xx,i} \;\; \sigma_{yy,i} \;\; \tau_{xy,i}]^{\mathrm{T}}$ is the stress at node i, and the basis polynomials (see Section 2.1) are

$$h_1^{(a,3)} = \tfrac{9}{2} a_1 \left(a_1 - \tfrac{1}{3}\right)\left(a_1 - \tfrac{2}{3}\right), \quad \text{etc.}$$

3.2.1 Continuum equilibrium

For strict intra-element equilibrium, the equation

$$\mathbf{E}\tilde{\boldsymbol{\sigma}} + \mathbf{b} = \mathbf{0} \qquad (7)$$

must hold throughout the element, where

$$\mathbf{E} = \begin{bmatrix} h_{1,x}^{(a,3)} & 0 & h_{1,y}^{(a,3)} & \cdots & h_{10,x}^{(a,3)} & 0 & h_{10,y}^{(a,3)} \\ 0 & h_{1,y}^{(a,3)} & h_{1,x}^{(a,3)} & \cdots & 0 & h_{10,y}^{(a,3)} & h_{10,x}^{(a,3)} \end{bmatrix}$$

and

$$\tilde{\boldsymbol{\sigma}} = [\sigma_{xx,1} \;\; \sigma_{yy,1} \;\; \tau_{xy,1} \;\; \cdots \;\; \sigma_{xx,10} \;\; \sigma_{yy,10} \;\; \tau_{xy,10}]^{\mathrm{T}}$$

The partial derivatives in $\mathbf{E}$ can be obtained in a similar way to that outlined for the cubic Bernstein stress element (Section 3.1.1), with the matrix $\mathbf{P}$ modified to contain the partial derivatives of the Lagrange basis polynomials with respect to the area coordinates. Again, there is a choice between enforcing Equation (7) directly at six suitably chosen points, or making 'Bernstein decompositions' of $\mathbf{E}$ and $\mathbf{b}$ and enforcing the constraints

$$\mathbf{E}_i^* \tilde{\boldsymbol{\sigma}} + \mathbf{b}_i^* = \mathbf{0} \quad \forall i \in \{1,\dots,6\}$$

Either method ensures strict equilibrium provided the variation of $\mathbf{b}$ is no more than quadratic.

3.2.2 Interface and boundary equilibrium

Referring once more to Figure 5, if the stress fields $\boldsymbol{\sigma}_{\mathrm{A}}$ and $\boldsymbol{\sigma}_{\mathrm{B}}$ have cubic Lagrange interpolations given by Equation (6), the traction vector $\mathbf{t}$ along each interface or boundary edge also has a cubic Lagrange interpolation, namely

$$\mathbf{t} = \sum_{i=1}^{4} h_i^{(l,3)} \mathbf{t}_i \qquad (8)$$

where $\mathbf{t}_i$ is the traction at node i, and

$$h_1^{(l,3)} = \tfrac{9}{2} l_1 \left(l_1 - \tfrac{1}{3}\right)\left(l_1 - \tfrac{2}{3}\right), \quad \text{etc.}$$

Since the variation is cubic, strict equilibrium along the whole edge can be ensured by enforcing equilibrium at each of the four nodes. The constraints take the form

$$\mathbf{E}_{\mathrm{A}} \boldsymbol{\sigma}_{\mathrm{A}i} + \mathbf{E}_{\mathrm{B}} \boldsymbol{\sigma}_{\mathrm{B}i} = \mathbf{0} \quad \forall i \in \{1,\dots,4\}$$

for an inter-element discontinuity, or

$$\mathbf{E}_{\mathrm{A}} \boldsymbol{\sigma}_{\mathrm{A}i} = \mathbf{t}_i \quad \forall i \in \{1,\dots,4\}$$

for a boundary edge where a surface traction field $\mathbf{t}$ (which can vary up to cubically) is prescribed.

3.2.3 *Continuum yield*

Lagrange basis polynomials do not provide a convex combination when $N \geq 2$ (they fail to satisfy the non-negativity condition), so for the cubic Lagrange stress element under consideration, applying a continuum yield restriction to each nodal stress does *not* guarantee that it will be satisfied for the interpolated stress:

$$f(\boldsymbol{\sigma}_i) \leq 0 \;\; \forall i \in \{1, \ldots, 10\} \quad \not\Rightarrow \quad f(\boldsymbol{\sigma}) \leq 0$$

To obtain a strict LB solution using elements of this type, it is possible to undertake a series of analyses in which additional yield constraints (at points other than the nodes) are introduced adaptively to suppress any yield violations and ensure that $f(\boldsymbol{\sigma}) \leq 0$ everywhere. This was done successfully by Hodge and Belytschko (1968) and Belytschko and Hodge (1970) in various LB analyses that used quadratic Lagrange stress elements. However, this method is difficult to implement robustly for Lagrange interpolations of arbitrary order N, and it does not appear to have been used since.

Another approach (cf. Pastor and Turgeman, 1982) is to perform a single 'LB' analysis in which violations of the yield restriction are permitted away from the nodes; a search is then conducted to find the point at which the worst violation occurs, and it is argued that the stress field (which does satisfy equilibrium) would be a true LB solution if the original material had its yield strength scaled up by an appropriate factor. In practice, this indirect method tends to give rather poor LB solutions.

3.2.4 *Interface yield*

Similarly, the use of Lagrange interpolation in Equation (8) means that applying an interface yield restriction to each nodal traction does *not* guarantee that it will be satisfied for the interpolated traction:

$$f(\mathbf{t}_i) \leq 0 \;\; \forall i \in \{1, \ldots, 4\} \quad \not\Rightarrow \quad f(\mathbf{t}) \leq 0$$

An exception is the case of a smooth interface, for which the yield restriction is an equality constraint specifying that no tangential traction can be sustained ($t_t = 0$).

4 PLANE STRAIN – UPPER BOUND

The 3-node (linear velocity, constant strain rate) triangle has been widely used to obtain strict UB solutions for plane strain problems since it was introduced by Pastor and Turgeman (1976) and Bottero et al. (1980).

Makrodimopoulos and Martin (2007, 2008) showed that strict UB solutions can be obtained using 6-node triangular elements with a quadratic Lagrange variation of velocity, and hence a linear variation of strain rate.

Makrodimopoulos (2022) showed that UB FELA can also be performed using Bernstein velocity elements, with no limit on the degree of polynomial interpolation, and with no difficulties arising from the (optional) inclusion of inter-element velocity discontinuities.

In this section, the use of higher-order triangular elements for UB FELA in plane strain will be illustrated in detail for a cubic ($N = 3$) variation of velocity. As such, attention will be focused on the 10-node triangle shown in Figure 2(d), considering both Bernstein and Lagrange interpolation schemes.

4.1 Higher-order velocity elements (Bernstein)

When cubic Bernstein interpolation is used, the velocity field $\mathbf{u} = [u_x \;\; u_y]^{\mathrm{T}}$ varies in accordance with

$$\mathbf{u} = \sum_{i=1}^{10} h_i^{(a,3)} \mathbf{u}_i^* \tag{9}$$

where $\mathbf{u}_i^* = [u_{x,i}^* \;\; u_{y,i}^*]^{\mathrm{T}}$ is the nodal velocity weight applied to the ith basis polynomial from the set

$$\boldsymbol{h}^{(a,3)} = \left\{ \begin{matrix} a_1^3, a_2^3, a_3^3, \\ 3a_1^2 a_2, 3a_1 a_2^2, 3a_2^2 a_3, 3a_2 a_3^2, 3a_3^2 a_1, 3a_3 a_1^2, \\ 6a_1 a_2 a_3 \end{matrix} \right\}$$

4.1.1 *Continuum strain rates*

The strain rate field $\boldsymbol{\varepsilon} = [\varepsilon_{xx} \;\; \varepsilon_{yy} \;\; \gamma_{xy}]^{\mathrm{T}}$ is obtained by differentiation of Equation (9), giving

$$\boldsymbol{\varepsilon} = \mathbf{B}\tilde{\mathbf{u}}^* \tag{10}$$

where

$$\mathbf{B} = \begin{bmatrix} h_{1,x}^{(a,3)} & 0 & \cdots & h_{10,x}^{(a,3)} & 0 \\ 0 & h_{1,y}^{(a,3)} & \cdots & 0 & h_{10,y}^{(a,3)} \\ h_{1,y}^{(a,3)} & h_{1,x}^{(a,3)} & \cdots & h_{10,y}^{(a,3)} & h_{10,x}^{(a,3)} \end{bmatrix}$$

and

$$\tilde{\mathbf{u}}^* = [u_{x,1}^* \;\; u_{y,1}^* \;\; \cdots \;\; u_{x,10}^* \;\; u_{y,10}^*]^{\mathrm{T}}$$

The partial derivatives in $\mathbf{B}$ can be obtained by forming the matrix $\mathbf{PQ}$ as described in Section 3.1.1. The operation of copying entries from the 10×2 matrix $\mathbf{PQ}$ to populate the 3×20 matrix $\mathbf{B}$ is denoted "$\mathrm{op_B}$":

$$\mathbf{B} = \mathrm{op_B}[\mathbf{PQ}] \tag{11}$$

The quadratic terms in $\mathbf{P}$ (and hence $\mathbf{B}$) indicate that, as expected, the strain rate varies quadratically (one degree lower than the cubic variation of velocity). For reasons that will become clear, it is desirable to express the variation of $\boldsymbol{\varepsilon}$ as a quadratic *Bernstein* variation. As shown in Section 3.1.1, $\mathbf{P}$ can be decomposed as

$$\mathbf{P} = a_1^2 \mathbf{P}_1^* + a_2^2 \mathbf{P}_2^* + a_3^2 \mathbf{P}_3^* + 2a_1 a_2 \mathbf{P}_4^* + 2a_2 a_3 \mathbf{P}_5^* + 2a_3 a_1 \mathbf{P}_6^*$$

Equation (11) can then be elaborated as

$$\mathbf{B} = a_1^2\mathbf{B}_1^* + a_2^2\mathbf{B}_2^* + a_3^2\mathbf{B}_3^* + 2a_1a_2\mathbf{B}_4^* + 2a_2a_3\mathbf{B}_5^* + 2a_3a_1\mathbf{B}_6^* \quad (12)$$

where

$$\mathbf{B}_i^* = \mathrm{op}_\mathrm{B}[\mathbf{P}_i^*\mathbf{Q}]$$

Substituting Equation (12) into Equation (10) shows that the strain rate field $\boldsymbol{\varepsilon} = [\varepsilon_{xx}\ \varepsilon_{yy}\ \gamma_{xy}]^\mathrm{T}$ varies in accordance with the quadratic Bernstein interpolation

$$\boldsymbol{\varepsilon} = \sum_{i=1}^{6} h_i^{(a,2)}\boldsymbol{\varepsilon}_i^* \quad (13)$$

where

$$\boldsymbol{\varepsilon}_i^* = [\varepsilon_{xx,i}^*\ \varepsilon_{yy,i}^*\ \gamma_{xy,i}^*]^\mathrm{T} = \mathbf{B}_i^*\tilde{\mathbf{u}}^* \quad (14)$$

is the strain rate weight applied to the *i*th basis polynomial from the set

$$\boldsymbol{h}^{(a,2)} = \{a_1^2, a_2^2, a_3^2, 2a_1a_2, 2a_2a_3, 2a_3a_1\}$$

Equation (13) shows that the strain rate $\boldsymbol{\varepsilon}$ at any point in the element can be expressed as a convex combination of six discrete strain rate weights $\boldsymbol{\varepsilon}_i^*$, each of which is obtained from a simple matrix-vector product involving $\mathbf{B}_i^*$ (a sparse matrix depending only on the coordinates of the element vertices) acting on $\tilde{\mathbf{u}}^*$ (the assembled vector of nodal velocity weights) in Equation (14). The strain rate weights $\boldsymbol{\varepsilon}_i^*$ can be viewed as sampling the quadratic variation of $\boldsymbol{\varepsilon}$ at the six derivative points shown in Figure 2(d). At the vertex derivative points the actual strain rate is equal to the corresponding weight ($\boldsymbol{\varepsilon}_i = \boldsymbol{\varepsilon}_i^*$ for $i = 1, 2, 3$), but at the mid-side derivative points the actual strain rate is a linear (in fact convex) combination of the three weights associated with that side (e.g. $\boldsymbol{\varepsilon}_4 = \frac{1}{4}\boldsymbol{\varepsilon}_1^* + \frac{1}{4}\boldsymbol{\varepsilon}_2^* + \frac{1}{2}\boldsymbol{\varepsilon}_4^*$).

The fact that Equation (13) expresses $\boldsymbol{\varepsilon}$ as a convex combination is the key to achieving global compliance with the flow rule when performing UB FELA with elements of this type. For any convex yield function, it can be shown that the set of plastically admissible strain rates – those satisfying the associated flow rule – is also convex (Salençon, 1977). This means that if a particular continuum flow rule is applied to each of the six strain rate weights $\boldsymbol{\varepsilon}_i^*$, it is guaranteed to be satisfied for the interpolated strain rate $\boldsymbol{\varepsilon}$ throughout the element, as required for a strict UB solution.

4.1.2 Continuum flow rule and dissipation

Taking the archetypal example of a Mohr–Coulomb material (cohesion c, friction angle ϕ) and assuming for the time being that $\phi > 0$, the continuum flow rule is

$$\varepsilon_{xx} + \varepsilon_{yy} \geq \sin\phi \cdot \sqrt{(\varepsilon_{xx} - \varepsilon_{yy})^2 + (\gamma_{xy})^2}$$

and the dissipation function is

$$D = c\cot\phi \cdot (\varepsilon_{xx} + \varepsilon_{yy})$$

As discussed by Makrodimopoulos and Martin (2007), it is convenient to recast these equations as

$$\varepsilon_{xx} + \varepsilon_{yy} = \sin\phi \cdot \lambda \quad (15a)$$

$$\lambda \geq \sqrt{(\varepsilon_{xx} - \varepsilon_{yy})^2 + (\gamma_{xy})^2} \quad (15b)$$

$$D = c\cos\phi \cdot \lambda \quad (15c)$$

To apply this formulation to the Bernstein element under consideration, the auxiliary variable λ is interpolated in the same way as the strain rate $\boldsymbol{\varepsilon}$ in Equation (13):

$$\lambda = \sum_{i=1}^{6} h_i^{(a,2)}\lambda_i^* \quad (16)$$

The flow rule is then applied to each strain rate weight $\boldsymbol{\varepsilon}_i^*$ and its corresponding λ_i^*, i.e. the constraints

$$\varepsilon_{xx,i}^* + \varepsilon_{yy,i}^* = \sin\phi \cdot \lambda_i^* \quad (17a)$$

$$\lambda_i^* \geq \sqrt{(\varepsilon_{xx,i}^* - \varepsilon_{yy,i}^*)^2 + (\gamma_{xy,i}^*)^2} \quad (17b)$$

are enforced for $i = 1, \ldots, 6$. As discussed above, this ensures that the interpolated strain rate $\boldsymbol{\varepsilon}$ satisfies the flow rule throughout the element, provided the friction angle ϕ is constant over the element (this will be assumed). The total dissipation over the element is

$$W_\mathrm{int} = \int c\cos\phi \cdot \lambda\, dA$$

In this integral the variation of λ is given by Equation (16), and $\cos\phi$ is constant. If c is also constant, the total dissipation is simply

$$W_\mathrm{int} = c\cos\phi \cdot \frac{A}{6} \cdot (\lambda_1^* + \cdots + \lambda_6^*) \quad (18)$$

since

$$\int h_i^{(a,2)} dA = \frac{A}{6} \quad \forall i \in \{1, \ldots, 6\}$$

Otherwise, the variation of c needs to be considered in conjunction with the (quadratic) variation of λ.

For a purely cohesive material (one with $\phi = 0$), the continuum flow rule is the constant volume condition

$$\varepsilon_{xx} + \varepsilon_{yy} = 0$$

and the dissipation function is

$$D = c \cdot \sqrt{\left(\varepsilon_{xx} - \varepsilon_{yy}\right)^2 + \left(\gamma_{xy}\right)^2} \qquad (19)$$

The approach above (Equation (15) onwards) can still be employed when $\phi = 0$. It is no longer guaranteed that the total dissipation over the element will be integrated exactly (as it is when $\phi > 0$), but the value obtained for W_{int} (e.g. from Equation (18)) will always be greater than or equal to the true dissipation, thus preserving the strictness of the UB solution.

The possibility of divergence between the calculated dissipation and the true dissipation arises because when the UB load multiplier β^+ is minimised in an analysis with $\phi = 0$, the inequality in Equation (15b) is only certain to become 'tight' at the finite number of derivative points where it is applied, via Equation (17b). At other points in the element, the inequality in Equation (15b) is still certain to be satisfied because it is convex, but it will not necessarily be satisfied tightly. This precludes exact integration of the cohesive dissipation function, Equation (19), at least during the optimisation process. If desired, exact (or highly accurate numerical) integration of Equation (19) can be performed as a post-processing task once the velocity field (and hence the strain rate field) for a given problem has been determined. This will generally lead to a marginal improvement (i.e. lowering) of the UB load multiplier that was obtained from the optimisation.

4.1.3 Interface velocity discontinuities

In UB FELA it is often beneficial to incorporate velocity discontinuities between some (or all) elements, rather than using a fully continuous velocity field. For each such velocity discontinuity, it is necessary to apply the interface flow rule and integrate the dissipation function, allowing for the possibility that up to three different materials may be involved – one for each of the adjacent solid elements, plus one for the interface itself.

Figure 6(a) shows a velocity discontinuity between two adjacent 2D elements, A and B, with a 1D element of the same order ($N = 3$) embedded along the interface (which has unit normal $\mathbf{n} = [n_x \; n_y]^{\mathrm{T}}$). If the velocity fields $\mathbf{u}_{\mathrm{A}}$ and $\mathbf{u}_{\mathrm{B}}$ have cubic Bernstein interpolations given by Equation (9), the velocity jump $\Delta\mathbf{u} = \mathbf{u}_{\mathrm{B}} - \mathbf{u}_{\mathrm{A}}$ also has a cubic Bernstein interpolation, namely

$$\Delta\mathbf{u} = \sum_{i=1}^{4} h_i^{(l,3)} \Delta\mathbf{u}_i^* \qquad (20)$$

where

$$\Delta\mathbf{u}_i^* = \mathbf{u}_{\mathrm{B}i}^* - \mathbf{u}_{\mathrm{A}i}^* \qquad (21)$$

and the basis polynomials are

$$h_1^{(l,3)} = l_1^3, \quad \text{etc.}$$

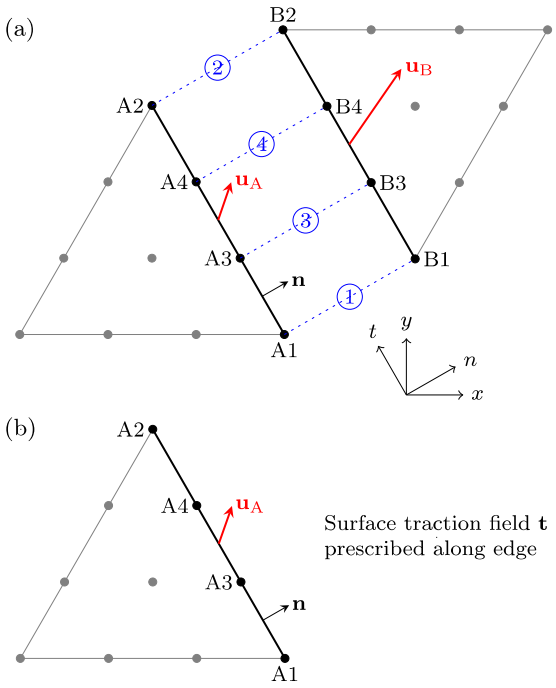

Figure 6. UB FELA with cubic interpolation of velocity: (a) inter-element discontinuity; (b) boundary edge

4.1.4 Interface flow rule and dissipation

For the example case of a Mohr–Coulomb material, assuming for the time being that $\phi > 0$ and that only a single material is involved, the interface flow rule is

$$\Delta u_n \geq \tan\phi \cdot |\Delta u_t|$$

and the dissipation function is

$$D = c \cot\phi \cdot \Delta u_n$$

where the local axes (n, t) are shown in Figure 6(a).

It is convenient, cf. Equation (15), to introduce an auxiliary variable μ and recast these equations as

$$\Delta u_n = \tan\phi \cdot \mu \qquad (22a)$$
$$\mu \geq |\Delta u_t| \qquad (22b)$$
$$D = c \cdot \mu \qquad (22c)$$

To apply this formulation to the Bernstein element under consideration, the auxiliary variable μ is interpolated in the same way as the velocity jump $\Delta\mathbf{u}$ in Equation (20):

$$\mu = \sum_{i=1}^{4} h_i^{(l,3)} \mu_i^* \qquad (23)$$

The flow rule is then applied to each nodal velocity jump weight $\Delta\mathbf{u}_i^*$ and its corresponding μ_i^*, i.e. the constraints

$$\Delta u_{n,i}^* = \tan\phi \cdot \mu_i^*$$
$$\mu_i^* \geq \left|\Delta u_{t,i}^*\right|$$

are enforced for $i = 1, \ldots, 4$, making use of

$$\begin{bmatrix}\Delta u^*_{n,i}\\ \Delta u^*_{t,i}\end{bmatrix} = \begin{bmatrix} n_x & n_y \\ -n_y & n_x\end{bmatrix}\begin{bmatrix}\Delta u^*_{x,i}\\ \Delta u^*_{y,i}\end{bmatrix}$$

where $\Delta u^*_{x,i}$ and $\Delta u^*_{y,i}$ are the components of $\Delta\mathbf{u}^*_i$ as determined from Equation (20). The interpolated velocity jump $\Delta\mathbf{u}$ satisfies the interface flow rule at every point along the interface, provided ϕ is constant. This is because Equations (20) and (23), cf. Equations (13) and (16), both define convex combinations. The total dissipation along the interface is

$$W_{\text{int}} = \int c\cdot\mu\, dL$$

In this integral the variation of μ is given by Equation (23). If c is constant, the total dissipation is simply

$$W_{\text{int}} = c\cdot\tfrac{L}{4}\cdot(\mu^*_1+\cdots+\mu^*_4)$$

in view of Equation (1a). Otherwise, the variation of c needs to be considered in conjunction with the (cubic) variation of μ.

For a purely cohesive material (one with $\phi = 0$), the interface flow rule is the tangential slip condition

$$\Delta u_n = 0$$

and the dissipation function is

$$D = c\cdot|\Delta u_t|$$

The approach above (Equation (22) onwards) can still be employed when $\phi = 0$. A strict UB solution is always obtained, but comments analogous to those made at the end of Section 4.1.2 apply once more.

Velocity jumps involving more than one material can also be handled easily.

4.1.5 Equivalent nodal loads

If Bernstein velocity elements are used to solve UB problems that involve body forces or surface tractions, it is necessary to determine the equivalent nodal forces $\mathbf{F}_i = [F_{x,i}\ \ F_{y,i}]^{\mathrm{T}}$ that are work-conjugate with the nodal velocity weights $\mathbf{u}^*_i = [u^*_{x,i}\ \ u^*_{y,i}]^{\mathrm{T}}$.

If a body force field $\mathbf{b} = [b_x\ \ b_y]^{\mathrm{T}}$ acts on the cubic Bernstein velocity element under consideration, the external work rate W_{ext} is obtained by integrating the scalar product $\mathbf{b}^{\mathrm{T}}\mathbf{u}$ over the area of the element, giving the components of $\mathbf{F}_i$ as

$$F_{x,i} = \int b_x h_i^{(a,3)} dA$$
$$F_{y,i} = \int b_y h_i^{(a,3)} dA$$

If $\mathbf{b}$ is constant, then in view of Equation (1b) the equivalent nodal forces are the same at all 10 nodes:

$$\begin{bmatrix}F_{x,i}\\ F_{y,i}\end{bmatrix} = \tfrac{A}{10}\begin{bmatrix}b_x\\ b_y\end{bmatrix}\quad \forall i\in\{1,\dots,10\}$$

If a prescribed surface traction field $\mathbf{t} = [t_x\ \ t_y]^{\mathrm{T}}$ acts on an edge of this element, the external work rate W_{ext} is obtained by integrating the scalar product $\mathbf{t}^{\mathrm{T}}\mathbf{u}$ over the length of the edge. It is convenient to consider a 1D Bernstein element embedded along the edge in question (see Figure 6(b)). The velocity along the edge has a cubic Bernstein interpolation, namely

$$\mathbf{u} = \textstyle\sum_{i=1}^{4} h_i^{(l,3)}\mathbf{u}^*_i$$

where $h_1^{(l,3)} = l_1^3$, etc., so the components of $\mathbf{F}_i$ (now using the edge-local node numbering $i = 1,\dots,4$) are

$$F_{x,i} = \int t_x h_i^{(l,3)} dL$$
$$F_{y,i} = \int t_y h_i^{(l,3)} dL$$

If the prescribed $\mathbf{t}$ is constant along the edge, then in view of Equation (1a) the equivalent nodal forces are

$$\begin{bmatrix}F_{x,i}\\ F_{y,i}\end{bmatrix} = \tfrac{L}{4}\begin{bmatrix}t_x\\ t_y\end{bmatrix}\quad \forall i\in\{1,\dots,4\}$$

For a linear traction variation $\mathbf{t} = l_1\mathbf{t}_1 + l_2\mathbf{t}_2$, where $\mathbf{t}_i$ is the traction at vertex i (of the 1D element), the equivalent nodal forces in the x direction are

$$\begin{bmatrix}F_{x,1}\\ F_{x,2}\\ F_{x,3}\\ F_{x,4}\end{bmatrix} = \tfrac{L}{20}\begin{bmatrix}4 & 1\\ 1 & 4\\ 3 & 2\\ 2 & 3\end{bmatrix}\begin{bmatrix}t_{x,1}\\ t_{x,2}\end{bmatrix}$$

and similarly for the y direction.

4.2 Higher-order velocity elements (Lagrange)

When cubic Lagrange interpolation is used, the velocity field $\mathbf{u} = [u_x\ \ u_y]^{\mathrm{T}}$ varies in accordance with

$$\mathbf{u} = \textstyle\sum_{i=1}^{10} h_i^{(a,3)}\mathbf{u}_i \qquad (24)$$

where $\mathbf{u}_i = [u_x\ \ u_y]^{\mathrm{T}}$ is the velocity at node i, and the basis polynomials (see Section 2.1) are

$$h_1^{(a,3)} = \tfrac{9}{2}a_1\left(a_1-\tfrac{1}{3}\right)\left(a_1-\tfrac{2}{3}\right),\quad \text{etc.}$$

4.2.1 Continuum strain rates

The strain rate field $\boldsymbol{\varepsilon} = [\varepsilon_{xx}\ \ \varepsilon_{yy}\ \ \gamma_{xy}]^{\mathrm{T}}$ is obtained by differentiation of Equation (24), giving

$$\boldsymbol{\varepsilon} = \mathbf{B}\tilde{\mathbf{u}}$$

where

$$\mathbf{B} = \begin{bmatrix} h_{1,x}^{(a,3)} & 0 & \cdots & h_{10,x}^{(a,3)} & 0 \\ 0 & h_{1,y}^{(a,3)} & \cdots & 0 & h_{10,y}^{(a,3)} \\ h_{1,y}^{(a,3)} & h_{1,x}^{(a,3)} & \cdots & h_{10,y}^{(a,3)} & h_{10,x}^{(a,3)} \end{bmatrix}$$

and

$$\tilde{\mathbf{u}} = [u_{x,1} \;\; u_{y,1} \;\; \cdots \;\; u_{x,10} \;\; u_{y,10}]^{\mathrm{T}}$$

The partial derivatives in $\mathbf{B}$ can be obtained in a similar way to that outlined for the cubic Bernstein velocity element, with the matrix $\mathbf{P}$ modified to contain the partial derivatives of the Lagrange basis polynomials with respect to the area coordinates. Again, it is possible to make a 'Bernstein decomposition' of $\mathbf{B}$, allowing the variation of the strain rate field $\boldsymbol{\varepsilon} = [\varepsilon_{xx} \;\; \varepsilon_{yy} \;\; \gamma_{xy}]^{\mathrm{T}}$ to be expressed as a quadratic Bernstein interpolation

$$\boldsymbol{\varepsilon} = \sum_{i=1}^{6} h_i^{(a,2)} \boldsymbol{\varepsilon}_i^*$$

where

$$\boldsymbol{\varepsilon}_i^* = [\varepsilon_{xx,i}^* \;\; \varepsilon_{yy,i}^* \;\; \gamma_{xy,i}^*]^{\mathrm{T}} = \mathbf{B}_i^* \tilde{\mathbf{u}}$$

4.2.2 Continuum flow rule and dissipation

Having expressed the strain rate field $\boldsymbol{\varepsilon}$ as a quadratic Bernstein interpolation (even though the velocity field $\mathbf{u}$ has a cubic Lagrange interpolation), application of the continuum flow rule and integration of the dissipation function can proceed exactly as described in Section 4.1.2, with no loss of rigour.

If $N = 2$ rather than $N = 3$, there is a quadratic Lagrange variation of velocity and a linear variation of strain rate; this formulation coincides with the 'simplex strain' element for UB FELA that was introduced by Makrodimopoulos and Martin (2007).

4.2.3 Interface velocity discontinuities

Referring once more to Figure 6(a), if the velocity fields $\mathbf{u}_{\mathrm{A}}$ and $\mathbf{u}_{\mathrm{B}}$ have cubic Lagrange interpolations given by Equation (24), the velocity jump $\Delta\mathbf{u} = \mathbf{u}_{\mathrm{B}} - \mathbf{u}_{\mathrm{A}}$ also has a cubic Lagrange interpolation, namely

$$\Delta\mathbf{u} = \sum_{i=1}^{4} h_i^{(l,3)} \Delta\mathbf{u}_i$$

where

$$\Delta\mathbf{u}_i = \mathbf{u}_{\mathrm{B}i} - \mathbf{u}_{\mathrm{A}i}$$

and the basis polynomials are

$$h_1^{(l,3)} = \tfrac{9}{2} l_1 \left(l_1 - \tfrac{1}{3}\right)\left(l_1 - \tfrac{2}{3}\right), \quad \text{etc.}$$

4.2.4 Interface flow rule and dissipation

Because the Lagrange basis polynomials in the set $\boldsymbol{h}^{(l,3)}$ do not provide a convex combination, it is not possible to apply the interface flow rule and integrate the dissipation function in the rigorous manner that was outlined in Section 4.1.4. One solution is to force the cubic variation of the velocity jump in Figure 6(a) to be linear, by imposing the ancillary constraints

$$\Delta\mathbf{u}_3 = \tfrac{2}{3}\Delta\mathbf{u}_1 + \tfrac{1}{3}\Delta\mathbf{u}_2$$
$$\Delta\mathbf{u}_4 = \tfrac{1}{3}\Delta\mathbf{u}_1 + \tfrac{2}{3}\Delta\mathbf{u}_2$$

The flow rule can then be applied at each end of the edge (i.e. to $\Delta\mathbf{u}_1$ and $\Delta\mathbf{u}_2$) and the dissipation can easily be integrated in a way that ensures a strict UB solution.

If $N = 2$ rather than $N = 3$, the quadratic Lagrange variation of the velocity jump can either be linearised, or handled directly by using a technique specific to that situation (Makrodimopoulos and Martin, 2008).

4.2.5 Equivalent nodal loads

For elements that use Lagrange interpolation of the velocity field, the evaluation of equivalent nodal loads is a familiar process; it is no different to the evaluation of equivalent nodal loads when Lagrange elements are used in the displacement finite element method.

5 OTHER PROBLEM GEOMETRIES

5.1 3D

The methodologies described in Sections 3 and 4 can all be extended to 3D in the obvious way, e.g. the cubic Bernstein velocity element suitable for UB FELA in 3D is a 20-node tetrahedron in which the velocity field

$$\mathbf{u} = \sum_{i=1}^{20} h_i^{(v,3)} \mathbf{u}_i^*$$

induces a strain rate field that can be expressed as

$$\boldsymbol{\varepsilon} = \sum_{i=1}^{10} h_i^{(v,2)} \boldsymbol{\varepsilon}_i^* \qquad (25)$$

where $\boldsymbol{\varepsilon}_i^* = \mathbf{B}_i^* \tilde{\mathbf{u}}^*$. To apply the continuum flow rule and integrate the dissipation function in 3D, the formulations given by Makrodimopoulos and Martin (2007) and Martin and Makrodimopoulos (2008) for various yield criteria can be used, ensuring that all auxiliary variables are interpolated in the same way as the strain rate $\boldsymbol{\varepsilon}$ in Equation (25).

5.2 Axial symmetry

For axisymmetric problems it is possible to obtain strict LB and UB solutions using FELA (see e.g. Pastor and Turgeman, 1982; Turgeman and Pastor, 1982), but the resulting formulations impose such stringent restrictions

on the stress and velocity fields that useful results can only be obtained for quite simple problems. To achieve good performance (e.g. reliable convergence of the load multipliers β^- and β^+ with mesh refinement) for a range of axisymmetric problems, it seems to be necessary to relax certain aspects of the implementation of the LB and UB theorems. These analyses no longer qualify as genuine FELA, but the solutions obtained from such quasi-LB and quasi-UB analyses can still be useful.

When performing LB FELA in axial symmetry, it is desirable to use elements with a Bernstein (rather than Lagrange) interpolation of the stress field. The reason is that for Bernstein elements of any order N, applying a (convex) continuum yield restriction to each nodal stress weight $\boldsymbol{\sigma}_i^* = [\sigma_{rr,i}^* \ \sigma_{zz,i}^* \ \sigma_{\theta\theta,i}^* \ \tau_{rz,i}^*]^{\mathrm{T}}$ guarantees that the yield restriction will be satisfied for the interpolated stress $\boldsymbol{\sigma} = [\sigma_{rr} \ \sigma_{zz} \ \sigma_{\theta\theta} \ \tau_{rz}]^{\mathrm{T}}$ throughout the element, and the same applies to interface yield. This is not the case if higher-order ($N \geq 2$) Lagrange stress elements are used (cf. Sections 3.2.3 and 3.2.4). Although strict equilibrium can be imposed on elements of either type, for good results it is preferable to enforce equilibrium at a reduced number of points, with violations being permitted elsewhere. The choice of these points should be guided by the principle that equilibrium must still be satisfied on average (i.e. in an integral sense over each element). For a triangular axisymmetric stress element of order N, this can be achieved by using the evaluation points from a Gaussian quadrature scheme that is exact for polynomials of degree N (e.g. for a 6-node triangular element, a 3-point Gauss scheme is required).

Similar difficulties arise when performing UB FELA in axial symmetry. Using either Bernstein or Lagrange interpolation of the velocity field, it is certainly possible to evaluate the axisymmetric strain rates and apply the flow rule strictly (as well as integrating the dissipation function in a way that guarantees a strict UB solution). For good results, however, it is preferable to apply the flow rule (and evaluate the dissipation function) at a reduced number of points, with violations being permitted elsewhere. The choice of these points should be guided by the principle that the flow rule must still be satisfied on average (i.e. in an integral sense over each element). In the case of a purely cohesive material, for example, the overall volume of each element should remain constant during the (infinitesimal) straining induced by the velocity field. For a triangular axisymmetric velocity element of order N, this can be achieved by using the evaluation points from a Gaussian quadrature scheme that is exact for polynomials of degree N (e.g. for a 6-node triangular element, a 3-point Gauss scheme is required). If the velocity field is discontinuous, using Bernstein interpolation is attractive because it allows velocity jumps of any order N to be treated simply and rigorously (cf. Section 4.1.4) without the need to impose ancillary linearisation constraints on the velocity jump (cf. Section 4.2.4).

6 IMPLEMENTATION

The stress and velocity elements described in this paper have been implemented in the author's FELA program OxLim. Users typically interact with the main program via a driver script that coordinates a sequence of limit analyses with calls to the open-source mesh generators Triangle (Shewchuk, 2002) or TetGen (Si, 2015) to perform adaptive mesh refinement based on the spatial distribution of the strain rate invariant

$$2\sqrt{J_2(\mathbf{e})} = \sqrt{2e_{ij}e_{ij}} \tag{26}$$

where $\mathbf{e}$ is the deviatoric strain rate tensor. Users can also specify a custom mesh (structured or unstructured). For the special case of constant-volume deformation in plane strain, the invariant in Equation (26) is equal to the maximum shear strain rate $\gamma_{\max}$, and the adaptivity algorithm reduces to that used by Martin (2009) and in various subsequent studies involving the application of adaptive FELA to undrained problems in plane strain (e.g. Martin, 2011; Martin and White, 2012; Mana et al., 2013; Griffiths and Martin, 2020). Figure 7 shows the final adaptive meshes for two of the four examples discussed below.

Currently, all numerical optimisation in OxLim is performed by calling the interior-point solver from the MOSEK optimisation package (MOSEK ApS, 2022).

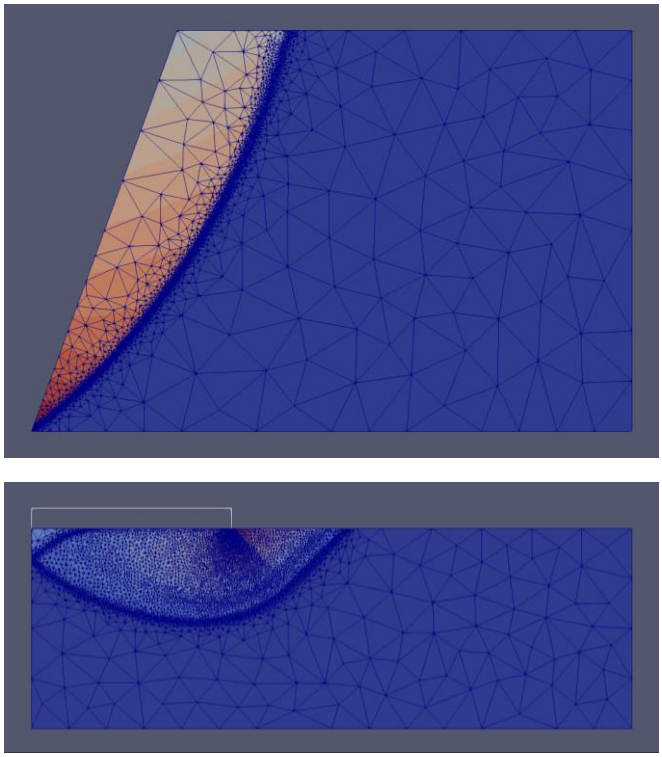

Figure 7. Final adaptively refined meshes for benchmark problems in Sections 6.2 (slope stability) and 6.3 (bearing capacity). Adaptive refinement performed using UB analyses with cubic Bernstein elements and continuous velocity fields. Strip footing analysis exploits symmetry (only right-hand half analysed). Contours show velocity magnitude

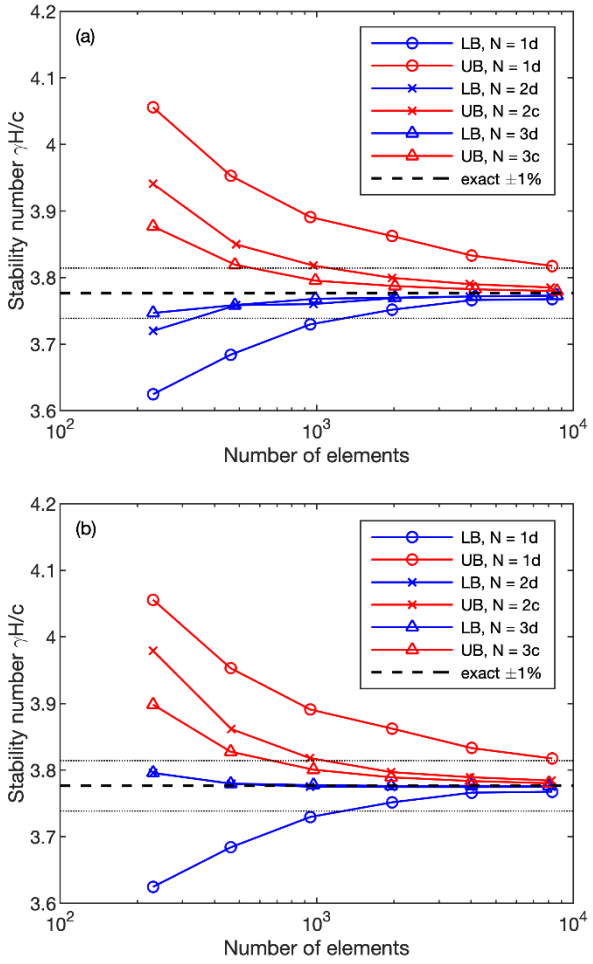

Figure 8. Adaptive analysis of plane strain vertical cut in Tresca soil using (a) Bernstein elements (b) Lagrange elements of various orders N (suffix indicates continuous or discontinuous stress/velocity field). Slip-line solution, presumed exact, is 3.776 (Martin, 2011)

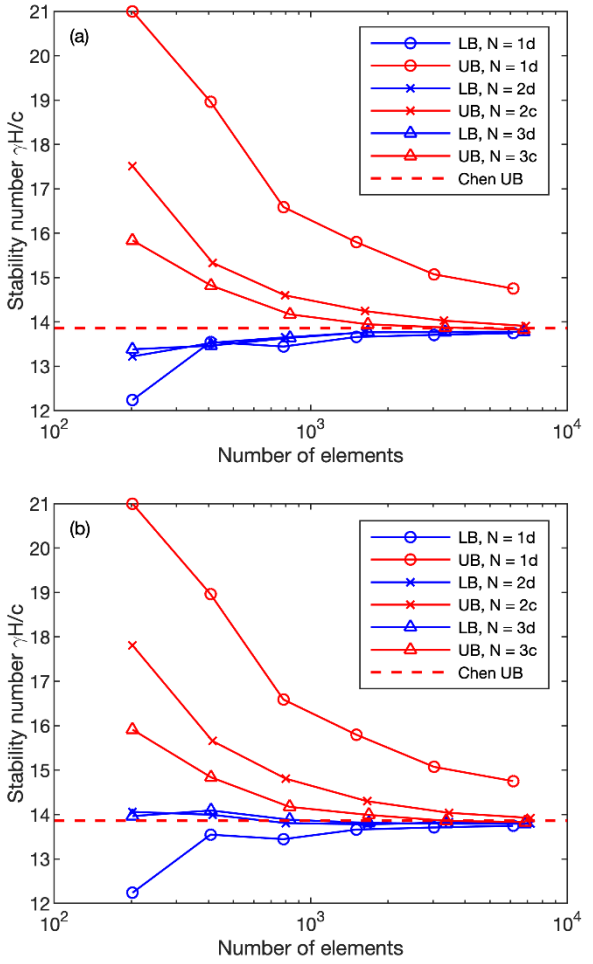

Figure 9. Adaptive analysis of plane strain 70° slope in Mohr–Coulomb soil ($\phi = 35°$) using (a) Bernstein elements (b) Lagrange elements of various orders N (suffix indicates continuous or discontinuous stress/velocity field). Reference UB solution from log-spiral mechanism is 13.86 (Chen, 1975)

6.1 Plane strain slope (Tresca)

The collapse of a plane strain vertical cut of height H in homogeneous Tresca soil (cohesion c, unit weight γ) was studied by Martin (2011) using the slip-line method, giving coincident LB and UB solutions (albeit without extension of the LB stress field) of $\gamma H/c = 3.776$. The FELA results in Figure 8 support the assertion that the slip-line solution is in fact exact. The use of adaptive meshing in conjunction with higher-order Bernstein elements (Figure 8(a)) provides strict LB and UB solutions with a bracketing error of ±0.1% from a mesh with fewer than 10 000 elements. When using Lagrange elements (Figure 8(b)), the UB solutions are strict for any order N, and they are very similar to the UB solutions obtained with Bernstein elements. However, the LB solutions obtained from higher-order Lagrange elements ($N \geq 2$) are not certain to be true lower bounds (see Section 3.2.3), and indeed with coarse meshes these 'LB' results are seen to be higher than the reference solution (which is a strict UB). Linear elements ($N = 1$) always give strict but relatively poor bounds, and these results are the same for both interpolation schemes.

6.2 Plane strain slope (Mohr–Coulomb)

A more challenging slope stability benchmark, at least for UB FELA, is the plane strain 70° slope in Mohr–Coulomb soil with $\phi = 35°$, previously studied by Makrodimopoulos and Martin (2007) among others. At present no exact solution from the slip-line method is available, but the strict UB solution of $\gamma H/c = 13.86$ obtained from a simple logarithmic spiral mechanism (Chen, 1975) turns out to be quite hard to improve. Figure 9(a) shows that adaptive meshing with cubic Bernstein velocity elements does eventually provide a strict UB solution that is slightly better than Chen's (13.83), using a mesh with fewer than 10 000 elements. For this problem, the UB results obtained using linear (3-node) velocity elements with discontinuities (denoted $N = 1\text{d}$) are markedly inferior to those obtained using higher-order elements with a continuous velocity field ($N = 2\text{c}$, $N = 3\text{c}$). Figure 9(b) is consistent with Figure 8(b); it indicates that if the mesh is sufficiently coarse, the 'LB' analyses conducted with higher-order ($N \geq 2$) Lagrange stress elements may give invalid results that exceed a known UB solution.

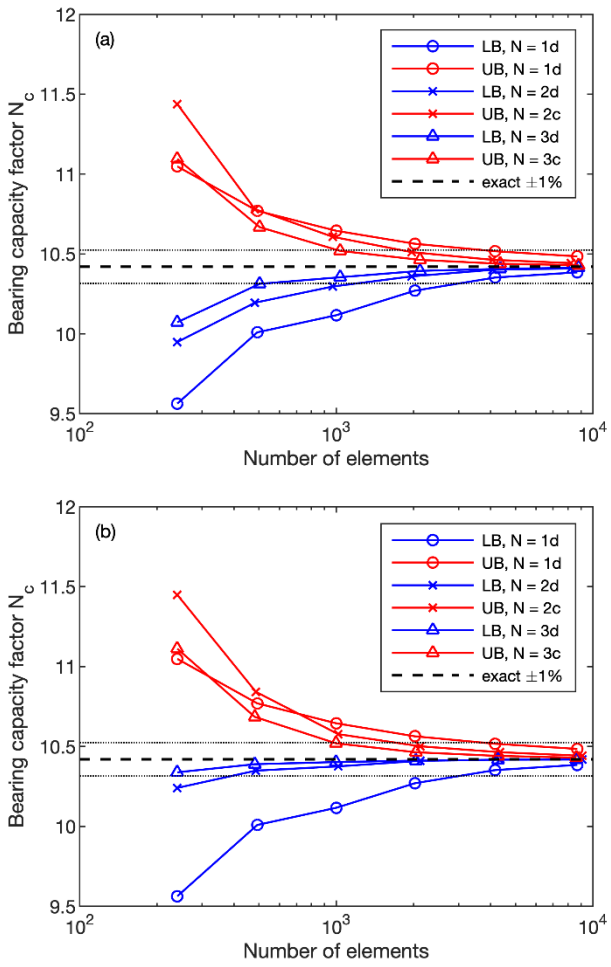

Figure 10. Adaptive analysis of rough strip footing on non-homogeneous Tresca soil ($\rho B/c_0 = 6$) using (a) Bernstein elements (b) Lagrange elements of various orders N (suffix indicates continuous or discontinuous stress/velocity field). Slip-line solution, presumed exact, is 10.42 (Martin, 2004)

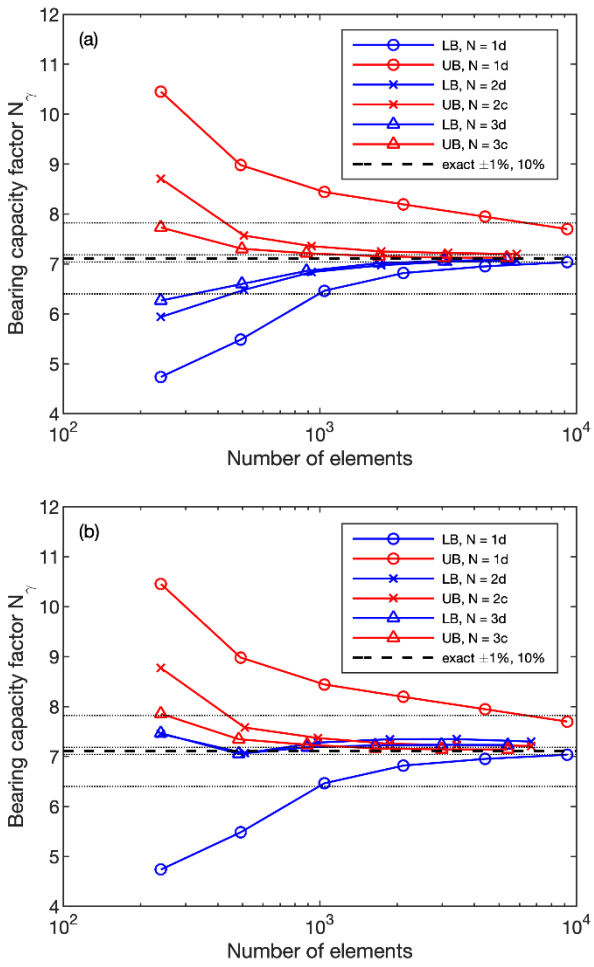

Figure 11. Adaptive analysis of smooth circular footing on Mohr–Coulomb soil ($c = 0,\ \phi = 30°$) using (a) Bernstein elements (b) Lagrange elements of various orders N (suffix indicates continuous or discontinuous stress/velocity field). Slip-line solution, presumed exact, is 7.111 (Martin, 2004)

6.3 Plane strain footing (Tresca)

This example concerns the bearing capacity of a rough strip footing of width B resting on a non-homogeneous Tresca soil with strength c_0 at the surface, increasing linearly with depth at a rate ρ. For the case $\rho B/c_0 = 6$, the cohesive bearing capacity factor N_c obtained from slip-line analysis using program ABC (Martin, 2004) is 10.42. The FELA results obtained using Bernstein elements of various orders are shown in Figure 10(a). The higher-order LB and UB solutions show rapid convergence to the slip-line solution. An oddity here is that for very coarse meshes (< 1000 elements), the UB results from linear elements are better than those from higher-order elements. This is possible because the linear elements also have velocity discontinuities included between all elements, whereas the higher-order elements use a continuous velocity field (on the grounds that with these elements, incorporating discontinuities has a minimal effect for fine unstructured meshes). In this example, the non-strict LB solutions obtained with higher-order Lagrange elements (Figure 10(b)) happen not to exceed the exact solution.

6.4 Axisymmetric footing (Mohr–Coulomb)

Accurate evaluation of the self-weight bearing capacity factor N_γ, which by definition pertains to the capacity of a surface foundation on cohesionless soil with friction angle ϕ and unit weight γ, has traditionally proven to be a difficult task for finite element methods. Here FELA is used to determine N_γ for a smooth circular footing on soil with $\phi = 30°$, taking the slip-line solution of 7.111 (Martin, 2004) as the reference value. Figure 11(a) shows that higher-order Bernstein elements perform well, reducing the bracketing error to ±0.3% using an adaptively refined mesh of less than 6000 elements. It is noticeable that linear velocity elements give poor UB solutions for this benchmark, despite the inclusion of velocity discontinuities (the final result is still about 8% high). From Figure 11(b) it is clear that higher-order Lagrange stress elements do not provide reliable LB solutions in this instance. Even as the mesh is refined, the 'LB' results for $N \geq 2$ remain above the slip-line solution and show no sign of converging to it. Strictly speaking, of course, none of the axisymmetric solutions in Figure 11 is a genuine LB or UB (see Section 5.2).

7 CONCLUSIONS

This paper has outlined the formulation of higher-order stress elements for LB FELA and higher-order velocity elements for UB FELA. It has been shown that, while it is possible to develop higher-order elements based on Lagrange polynomials (familiar from the displacement finite element method), elements that use an alternative interpolation scheme based on Bernstein polynomials have many advantages, particularly for LB FELA, where previously it has been difficult to ensure that the stress field satisfies the yield restriction at every point of a higher-order stress element.

It has been shown that, when combined with a simple algorithm for adaptive mesh refinement, higher-order stress and velocity elements can provide LB and UB collapse loads that bracket the exact solution with a high degree of accuracy for a range of benchmark problems. Further work is required to assess whether the use of higher-order elements does actually provide a net benefit (compared with the use of linear elements) in terms of accuracy for a given computation time, when solving various 2D and 3D limit analysis problems that are of interest in geotechnical engineering.

8 REFERENCES

Belytschko, T., Hodge, P.G. 1970. Plane stress limit analysis by finite elements, *J. of the Engineering Mechanics Division (ASCE)* **96**, 931–944.

Bottero, A., Negre, R., Pastor, J., Turgeman, S. 1980. Finite element method and limit analysis theory for soil mechanics problems, *Computer Methods in Applied Mechanics and Engineering* **22**, 131–149.

Chen, W.F. 1975. *Limit Analysis and Soil Plasticity*, Elsevier.

Cook, R.D., Malkus, D.S., Plesha, M.E., Witt, R.J. 2002. *Concepts and Applications of Finite Element Analysis*, Wiley.

Drucker, D.C., Prager, W., Greenberg, H.J. 1952. Extended limit design theorems for continuous media, *Quarterly of Applied Mathematics* **9**, 381–389.

Farouki, R.T. 2012. The Bernstein polynomial basis: a centennial retrospective, *Computer Aided Geometric Design* **29**, 379–419.

Griffiths, D.V., Martin, C.M. 2020. Critical failure mechanisms in relatively flat undrained slopes, *Géotechnique Letters* **10**, 95–99.

Hodge, P.G., Belytschko, T., 1968. Numerical methods for the limit analysis of plates, *J. of Applied Mechanics* **35**, 796–802.

Lai, M.-J., Schumaker, L.L. 2007. *Spline Functions on Triangulations*, Cambridge University Press.

Lysmer, J. 1970. Limit analysis of plane problems in soil mechanics, *J. of the Soil Mechanics and Foundations Division (ASCE)* **96**, 1311–1334.

Makrodimopoulos, A. 2020. A fundamental class of stress elements in lower bound limit analysis, *Proceedings of the Royal Society A* **476**:20200425.

Makrodimopoulos, A. 2022. A class of strain-displacement elements in upper bound limit analysis, *Int. J. for Numerical Methods in Engineering* **123**:3681–3712.

Makrodimopoulos, A., Martin, C.M. 2006. Lower bound limit analysis of cohesive-frictional materials using second-order cone programming, *Int. J. for Numerical Methods in Engineering* **66**, 604–634.

Makrodimopoulos, A., Martin, C.M. 2007. Upper bound limit analysis using simplex strain elements and second-order cone programming, *Int. J. for Numerical and Analytical Methods in Geomechanics* **31**, 835–865.

Makrodimopoulos, A., Martin, C.M. 2008. Upper bound limit analysis using discontinuous quadratic displacement fields, *Communications in Numerical Methods in Engineering* **24**, 911–927.

Mana, D.S.K., Gourvenec, S., Martin, C.M. 2013. Critical skirt spacing for shallow foundations under general loading, *J. of Geotechnical and Geoenvironmental Engineering* **139**, 1554–1566.

Martin, C.M. 2004. *User guide for ABC – Analysis of Bearing Capacity, Version 1.0*, OUEL Report No. 2261/03.

Martin, C.M. 2009. Undrained collapse of a shallow plane-strain trapdoor, *Géotechnique* **59**, 855–863.

Martin, C.M. 2011. The use of adaptive finite-element limit analysis to reveal slip-line fields, *Géotechnique Letters* **1**, 23–29.

Martin, C.M., Makrodimopoulos, A. 2008. Finite-element limit analysis of Mohr–Coulomb materials in 3D using semidefinite programming, *J. of Engineering Mechanics* **134**, 339–347.

Martin, C.M., White, D.J. 2012. Limit analysis of the undrained bearing capacity of offshore pipelines, *Géotechnique* **62**, 847–863.

MOSEK ApS 2022. *The MOSEK Optimizer API for C Manual, Version 9.3*, https://www.mosek.com

Pastor, J. 1978. Analyse limite: détermination numérique de solutions statiques complètes. Application au talus vertical, *J. de Mécanique Appliquée* **2**, 167–196.

Pastor, J., Turgeman, S. 1976. Mise en oeuvre numérique des méthodes de l'analyse limite pour les matériaux de von Mises et de Coulomb standards en déformation plane, *Mechanics Research Communications* **3**:469–476.

Pastor, J., Turgeman, S. 1982. Limit analysis in axisymmetrical problems: numerical determination of complete statical solutions, *Int. J. of Mechanical Sciences* **24**, 95–117.

Prautzsch, H., Boehm, W., Paluszny, M. 2002. *Bézier and B-Spline Techniques*, Springer.

Salençon, J. 1977. *Applications of the Theory of Plasticity in Soil Mechanics*, Wiley.

Salençon, J. 1983. *Calcul à la Rupture et Analyse Limite*, Presses de ENPC.

Shewchuk, J.R. 2002. Delaunay refinement algorithms for triangular mesh generation, *Computational Geometry* **22**, 21–74.

Si, H. 2015. TetGen, a Delaunay-based quality tetrahedral mesh generator, *ACM Transactions on Mathematical Software* **41**, Article No. 11, 1–36.

Turgeman, S., Pastor, J. 1982. Limit analysis: a linear formulation of the kinematic approach for axisymmetric mechanic problems, *Int. J. for Numerical and Analytical Methods in Geomechanics* **6**, 109–128.

Zienkiewicz, O.C., Taylor, R.L., Zhu, J.Z. 2005. *The Finite Element Method: Its Basis and Fundamentals*, Elsevier.